ALIGNMENT OF OUTFLOWS WITH MAGNETIC FIELDS IN CLOUD CORES

Tomoaki Matsumoto[1], Takeshi Nakazato[2,3], and Kohji Tomisaka[4]
Accepted by the Astrophysical Journal Letters

ABSTRACT

We estimate the polarized thermal dust emission from MHD simulations of protostellar collapse and outflow formation in order to investigate alignment of outflows with magnetic fields. The polarization maps indicate that alignment of an outflow with the magnetic field depends on the field strength inside the cloud core; the direction of the outflow, projected on the plane of the sky, is aligned preferentially with the mean polarization vector for a cloud core with a magnetic field strength of 80 μG, while it does not tend to be aligned for 50 μG as long as the 1000 AU scale is considered. The direction of the magnetic field at the cloud center is probed by the direction of the outflow. In addition, the magnetic field at the cloud center can be revealed by *ALMA* even when the source is embedded deeply in the envelope. The Chandrasekhar-Fermi formula is examined using the polarization maps, indicating that the field strength predicted by the formula should be corrected by a factor of $0.24 - 0.44$. The correction factor has a tendency to be lower for a cloud core with a weaker magnetic field.

Subject headings: ISM: clouds — ISM: jets and outflows — MHD — stars: formation — polarization

1. INTRODUCTION

Magnetic fields are believed to control not only protostellar collapse, but also formation of circumstellar disks and outflows. Many observations have suggested that the outflow and jet axis of the young star is aligned preferentially along the cloud-scale magnetic field (e.g., Cohen, Rowland, & Blair 1984; Strom et al. 1986; Vrba et al. 1986; Vrba, Strom, & Strom 1988; Tamura & Sato 1989; Jones & Amini 2003).

However, recent observations indicate a suggestion contrary to previous ones concerning the issue of alignment of outflows and jets with the magnetic fields. High-resolution observations of submillimeter polarization have resolved the magnetic fields around young stars on a $\sim 10^{3-4}$ AU scale, which is comparable to the outflow scale (Momose et al. 2001; Henning et al. 2001; Wolf, Launhardt, & Henning 2003; Vallée, Greaves, & Fiege 2003). Wolf et al. (2003) investigate alignment of outflows with magnetic fields for Bok globules associated with Class 0 protostars and Class I sources, suggesting that two Bok globules are associated with outflows parallel to the magnetic fields, while the two other globules are associated with outflows perpendicular to the magnetic fields. For Classical T Tauri stars (CTTSs), Ménard & Duchêne (2004) estimate orientation of the symmetry axes of the disk-jet systems in the Taurus-Auriga region, and indicate that CTTSs are oriented randomly with respect to the local magnetic field.

Recently, Matsumoto & Tomisaka (2004) (hereafter MT04) have performed MHD simulations of the collapse of magnetized cloud cores and reproduced outflow generation in order to investigate the directions of outflows,

circumstellar disk, rotation, and magnetic fields. The simulations show that the outflow tends to be aligned with a local magnetic field of a 10 AU scale irrespective of the magnetic field strength assumed, while the alignment depends on the field strength on the cloud core scale. A disk-outflow system is aligned with the cloud core scale magnetic field within $\sim 5°$ and $\sim 30°$ for the initial field strengths of 37.1 and 18.6 μG, respectively, because of the strong magnetic braking during the collapse. When a weak field strength of 7.42 μG is assumed, the outflow is not aligned with the cloud core scale magnetic field. In this Letter, alignment of an outflow with magnetic field is discussed by constructing polarization maps from the MHD simulations of MT04.

2. CLOUD MODEL AND POLARIZED EMISSION

Polarization of dust emission is calculated from MT04 MHD simulation data. The simulations follow the gravitational collapse of cloud cores, formation of a first stellar core (Larson 1969), and the launch of an outflow, resolving both the whole cloud core and the protostar. Polarization maps are constructed by extracting the central cubic region $(9128 \text{ AU})^3$ from all the simulation data.

The initial model of a cloud core is a slowly rotating, spherical, isothermal cloud threaded by a uniform magnetic field. The initial cloud core has the density profile of a Bonnor-Ebert sphere (Ebert 1955; Bonnor 1956), and the present model can be applied to Bok globules because Bok globules are thought to have Bonnor-Ebert density profiles (Alves et al. 2001; Harvey et al. 2001; Racca, Gómez, & Kenyon 2002). The initial central density is set as $\rho_0 = 1 \times 10^{-19} \text{ g cm}^{-3}$, which corresponds to a number density of $n_0 = 2.61 \times 10^4 \text{ cm}^{-3}$ for the assumed mean molecular weight of 2.3. The initial temperature of the gas is 10 K, the edge of the cloud is located at $r = 0.178$ pc from the center, and the mass of the cloud is $6.130 \, M_\odot$. The initial angular velocity is assumed to be $7.11 \times 10^{-7} \text{ yr}^{-1}$. In this Letter, the last stages of two models of MT04, models MF45 and WF45, are shown. In these models, the initial magnetic field is inclined at an angle of $\theta = 45°$ from the initial rota-

[1] Department of Humanity and Environment, Hosei University, Fujimi, Chiyoda-ku, Tokyo 102-8160, Japan, matsu@i.hosei.ac.jp
[2] National Astronomical Observatory, Mitaka, Tokyo 181-8588, Japan, nakazato@nro.nao.ac.jp
[3] Institut de Radioastronomie Millimétrique, 300 rue de la Piscine, 38406 Saint Martin d'Hères, France
[4] Division of Theoretical Astrophysics, National Astronomical Observatory, Mitaka, Tokyo 181-8588, Japan, tomisaka@th.nao.ac.jp

TABLE 1
Parameters and Properties of Model Cores

Models	B_0 (μG)	$\bar{B}$ (μG)	$\bar{n}$ (cm^{-3})	ϕ_{3D} (deg)
MF45	18.6	82.8	2.74×10^5	12.4
WF45	7.42	50.1	2.78×10^5	53.5

tion axis, which corresponds to the z-axis. The initial magnetic field strengths B_0 are shown in Table 1.

Table 1 also shows the mean strength of magnetic field $\bar{B}$ and mean number density $\bar{n}$ within the region $(9128 \text{ AU})^3$ for comparison with polarization maps in § 3. The mean values $\bar{B}$ and $\bar{n}$ are considerably larger than the initial values B_0 and n_0 because of amplification due to collapse. Angle ϕ_{3D} denotes a three-dimensional angle between the direction of the mean magnetic field within $r \leq 50$ AU and that within 4555 AU, indicating change in the direction of the magnetic field inside the cloud core (see Figs. 7 and 15 of MT04 for models MF45 and WF45, respectively), and model WF45 shows an angle larger than that in model MF45 because of the weak magnetic braking. The direction of the mean magnetic field within $r \leq 50$ AU approximately coincides with the local direction of the outflow, and is adopted here as an index of the direction of the outflow.

The polarization of dust emission is calculated following the analysis of Fiege & Pudritz (2000) and Padoan et al. (2001). As these studies do, we focus on the thermal dust emission at submillimeter wavelengths, neglecting scattering. The Stokes parameters Q and U are proportional to the following integrals of q and u when we assume that the grain properties and temperature are constant:

$$q = \int \rho \cos 2\psi \cos^2 \gamma \, ds, \qquad (1)$$

$$u = \int \rho \sin 2\psi \cos^2 \gamma \, ds, \qquad (2)$$

where the integrals $\int ds$ are performed along the line of sight, ρ denotes the gas density, ψ is the angle between the projection of the magnetic field on the plane of the sky and the north, and γ is the angle between the plane of the sky and the local direction of the magnetic field. The polarization angle χ is given by $\tan 2\chi = u/q$, where $-\pi/2 \leq \chi < \pi/2$. The polarization vector with χ traces the polarization shown by the B-vector of the submillimeter thermal emission, which is parallel to the interstellar magnetic field on the plane of the sky. The degree of polarization is calculated by $P = \alpha (q^2 + u^2)^{1/2} / (\Sigma - \alpha \Sigma_2)$ with $\Sigma = \int \rho \, ds$ and $\Sigma_2 = (1/2) \int \rho (\cos^2 \gamma - 2/3) \, ds$, where α is a parameter specified by the grain properties, and we adopt a constant value of $\alpha = 0.15$ following Padoan et al. (2001).

3. RESULTS

3.1. Polarization Maps of the Cloud Cores

Figure 1 shows the polarization maps overlaid by the surface density for models MF45 and WF45 for three orthogonal lines of sight (x, y, and z-directions). The elliptical distribution of the surface density reflects the flat

infalling envelope for all the models and for all the lines of sight (see Fig. 2 of MT04 for the three-dimensional density and magnetic field structures of model MF45). The hourglass structure of magnetic fields in three dimensions is projected directly on the polarization vector. The orientations of the mean polarization vector (thick green line) are perpendicular to the long axes of the surface densities. The degree of polarization along the long axis is less than that along the short axis due to the hourglass structure of the field lines; this field structure increases the component of the magnetic field parallel to the line of sight B_{los} compared with the perpendicular component $B_\perp$, and reduces the degree of polarization along the flat envelope.

The outflows are hardly visible in the maps because the outflows are extended up to only ~ 200 and 150 AU for models MF45 and WF45. We adopt here the direction of the mean magnetic field within $r \leq 50$ AU as an index of the direction of the outflow (thick red line). The projected direction of the outflow is almost aligned with the mean polarization vector (thick green line) for model MF45 irrespective of the lines of sight (Fig. 1a-c) because of a small intrinsic angle between the outflow and the cloud core scale magnetic field ($\phi_{3D} = 12.4°$). On the other hand, the alignment depends on the line-of-sight for model WF45 (Fig. 1d-f) because the outflow is not aligned with the magnetic field intrincically ($\phi_{3D} = 53.5°$). When model WF45 is observed along the x-direction (Fig. 1d), the projected direction of the outflow is aligned with the mean polarization vector by chance. They are not aligned considerably when observed along the y- and z-directions as shown in Figure 1e and 1f.

More qualitatively, Table 2 shows ϕ_{prj}, which is defined as an angle between the red and thick green lines. This angle indicates that the direction of the outflow tends to be aligned with the mean polarization vector on the plane of the sky when a cloud core has a strong magnetic field of $\bar{B} \sim 80\mu$G.

The polarization maps examined here demonstrate that the direction of the magnetic field at the cloud center can not be inferred from the polarization on the scale of this map ($\sim 10^3$ AU scale). Model MF45 shows polarization maps similar to model WF45, although the magnetic field at the cloud center of Model MF45 is projected to quite different direction from that of Model WF45.The directions of the central magnetic field reflect the those of outflows. In other words, the direction of the outflow probes the direction of the magnetic field at the cloud center.

Figure 2 simulates direct observations toward the cloud center on the 100 AU scale with high resolution of 25 AU for the three lines of sight for model WF45. These maps are constructed by convolution of the polarization pattern of Figure 1d–1f with a Gaussian beam of FWHM = 25 AU, which corresponds to angular resolution of $0.1''$ for an object at a distance of 250 pc, e.g., an observation toward B335 by *ALMA*. In constructing Figure 2, the envelope of 9128 AU scale is taken into account similar to Figure 1d–1f. On the scale of Figure 2, the polarization reveals the convergence of alignment between the disk-outflow system and the magnetic field; nevertheless the protostar is embedded deeply in the envelope. Figure 2 shows the polarization depending on the lines of
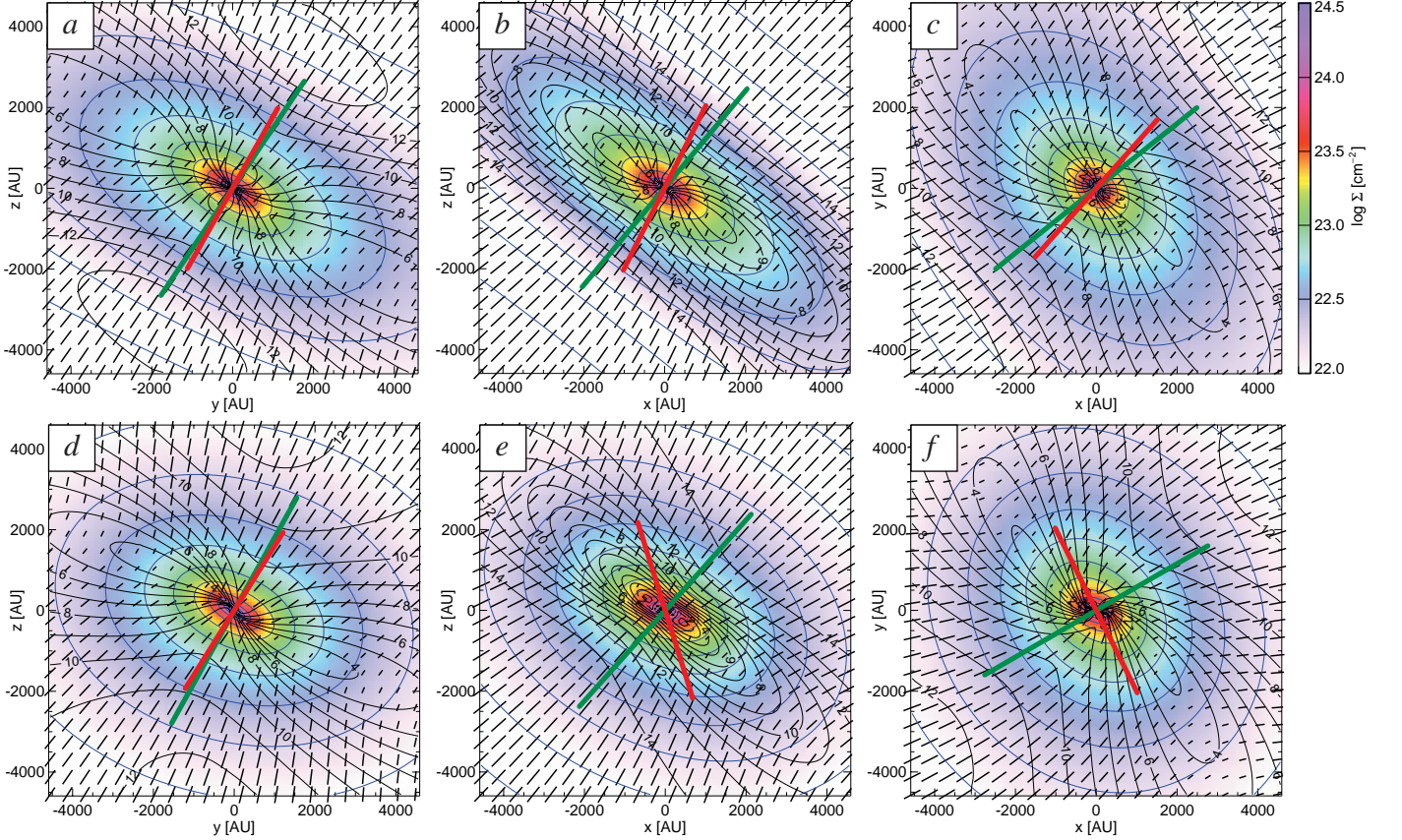
FIG. 1.— Polarization maps constructed from MHD data of the central (9182 AU)^3 box for models (*a-c*) MF45 and (*d-f*) WF45 along the lines of sight parallel to (*a, d*) the *x*-axis, (*b, e*) the *y*-axis, (*c, f*) and the *z*-axis, respectively. Vector traces the B-vector of the polarized thermal emission, and is therefore parallel to the interstellar magnetic field lines on the plane of the sky. The length of the vector is proportional to the degree of polarization, which is also shown by black contours at 1 % intervals. The mean orientation of the polarization vector is denoted by the thick green line. Color scale and blue contours denote the surface density Σ, which is proportional to the intensity of thermal dust emission when the gas is assumed to be optically thin. Thick red line denotes the projected direction of the mean magnetic fields averaged over $r \leq 50$AU, indicating the direction of the outflow.

TABLE 2
OUTFLOW ORIENTATIONS AND ESTIMATE OF MAGNETIC FIELD STRENGTHS

Models	Line of Sight	ϕ_{prj} (deg)	$\bar{\rho}$ (g cm^{-3})	δv (km s^{-1})	σ_χ (deg)	B_{CF} (μG)	f
MF45	x	4.40	1.04×10^{-18}	0.209	10.3	242.8	0.34
MF45	y	13.1	1.04×10^{-18}	0.214	11.0	233.2	0.35
MF45	z	9.62	1.04×10^{-18}	0.193	12.4	186.4	0.44
WF45	x	-3.02	1.06×10^{-18}	0.262	16.0	197.6	0.25
WF45	y	59.1	1.06×10^{-18}	0.251	14.3	212.2	0.24
WF45	z	86.5	1.06×10^{-18}	0.244	17.2	171.6	0.29

sight (see also Fig. 13 of MT04 for the three-dimensional structure). Figure 2*a* shows an edge-on view of the disk as reproducing the considerably flat surface density, and the polarization vector is almost perpendicular to the long axis of the surface density. The bipolar outflow is extended up to 150 AU vertically on the map, although it is hardly visible in both the polarization and the surface density. Figure 2*b* also shows an edge-on view, exhibiting a polarization pattern different from Figure 2*a*; the polarization vector is oriented along the projected disk surface because the radial component of the magnetic field in the hourglass structure contributes $B_\perp$ there. In $|z| \gtrsim 100$ AU, the polarization vector is still perpendicu-

lar to the disk, similar to Figure 2*a*. Figure 2*c* shows the change in the direction of the mean magnetic field; the outflow, whose direction is indicated by the thick line, is aligned with the central polarization vector.

3.2. *Estimate of Field Strengths from Polarization Maps*

Magnetic field strength can be estimated from the polarization maps of Figure 1 using the method of Chandrasekhar & Fermi (1953):

$$B_{\mathrm{CF}} = \left(\frac{4\pi}{3}\bar{\rho}\right)^{1/2} \frac{\delta v}{\sigma_\chi}, \qquad (3)$$
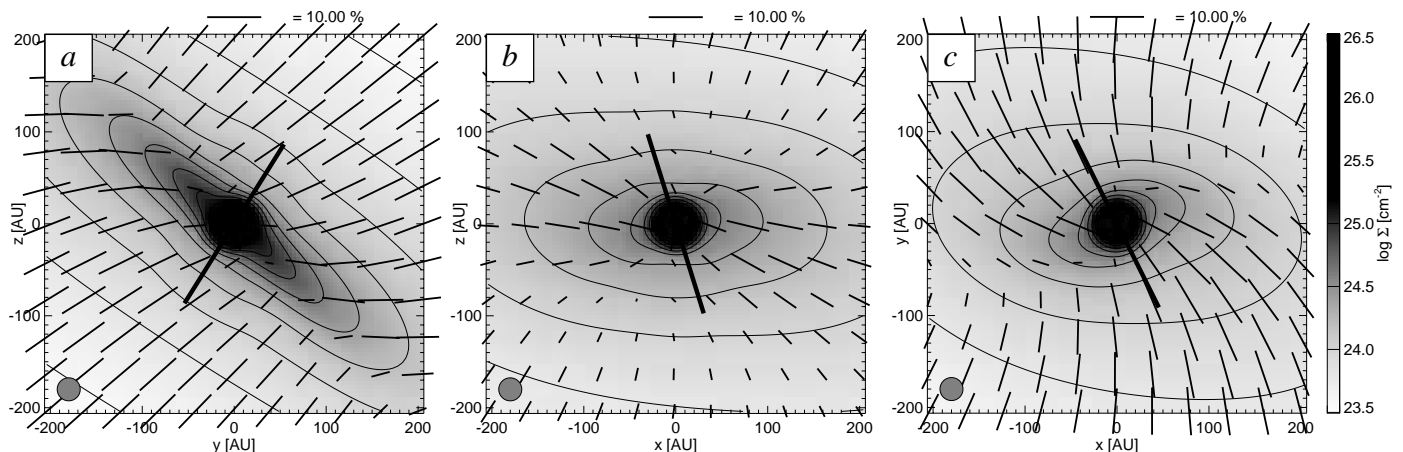
Fig. 2.— Polarization maps convoluted by the Gaussian beam with FWHM = 25AU toward the cloud center for model WF45 along the lines of sight parallel to (a) the x-axis, (b) the y-axis, and (c) the z-axis. The beam pattern is denoted in the bottom left corner of each panel. Thick line denotes the projected direction of the mean magnetic fields averaged over $r \leq 50$AU, indicating the direction of the outflow. Grayscale and contours denote the surface density.

where $\bar{\rho}$ denotes the mean density, estimated by averaging the surface density over the map, δv denotes the rms gas velocity, assumed as the velocity component parallel to the line of sight superposed as $\delta v^2 = \int \rho v_{\rm los}^2 dV / \int \rho dV$, and σ_χ denotes the standard deviation to the mean orientation angle of the polarization vector. The derived parameters $\bar{\rho}$, δv, σ_χ, and the estimated magnetic field strength $B_{\rm CF}$ are shown in Table 2 for the three orthogonal lines of sight.

The estimated field strengths range from 186 to 242 μG for model MF45, and from 171 to 212 μG for model WF45, exhibiting significant dispersion[5]. Moreover, these field strengths are $2-4$ times larger than the mean magnetic field strengths $\bar{B}$ (see Table 1), which are obtained directly from MHD data. In other words, the prediction of the Chandrasekhar-Fermi formula should be corrected by a factor of $f = 0.34 - 0.44$ for model MF45 and $f = 0.24 - 0.29$ for model WF45, as shown in Table 2. Ostriker, Stone, & Gammie (2001) and Padoan et al. (2001) also report such an overestimated field strength in application of the Chandrasekhar-Fermi formula, and obtain a correction factor of $f \simeq 0.4 - 0.5$, which is consistent with our case. Padoan et al. (2001) discuss the deviation from the prediction of the Chandrasekhar-Fermi formula as being attributable to deviation from the linear theory, which is assumed by Chandrasekhar & Fermi (1953). The large values of σ_χ shown in Table 2 indicate that the Alfvén wave is nonlinear with large amplitude in our models. Moreover, it is noteworthy that model WF45 exhibits larger σ_χ than model MF45, indicating that the correction is more significant for a cloud with weaker magnetic field.

4. DISCUSSION

Activity of an outflow may be discussed in terms of alignment of the outflow with the magnetic field. The cloud core with stronger magnetic field exhibits a faster outflow as shown in Figure 18 of MT04, and the outflow tends to be aligned with the polarization vector.

This indicates that the fast outflow is observed parallel to the magnetic field. According to the observations toward CTTSs, Ménard & Duchêne (2004) suggest a similar tendency in spite of the different evolutionary stage from that considered here: CTTSs without bright and extended outflows have a tendency to be perpendicular to the magnetic field.

The outflows are extended up to only $150 - 200$ AU in the MHD simulation data used here, while the outflows observed by molecular line emission are extended up to a 1000 AU scale (e.g., Wolf et al. 2003). Moreover, the outflows presented here have considerably slower velocity than that observed around young stars. Therefore the cloud cores presented here are restricted to the very early evolutionary stage compared with the observed cloud cores. This restriction arises in response to computational cost for solving the launch mechanism of the outflow near the protostar. In further stages, the magnetic field hardly seems to affect the direction of the outflow on the scale of 1000 AU, because the outflow is accelerated at $r \sim 10$ AU at a speed comparable to the Alfvén velocity at this radius, and the magnetic field strength of the envelope decreases rapidly, proportional to $B \propto r^{-1}$. Moreover, the protostar may be decoupled from the magnetic field of the envelope as a result of efficient ambipolar diffusion (Nakano, Nishi, & Umebayashi 2002) in further stages. The directions of the outflow will be fixed during the main accretion phase of the protostar.

[5] We confirmed that a method proposed by Houde (2004) can correct a projection effect of the magnetic field.

REFERENCES

Alves, J., Lada, C. J., & Lada, E. A. 2001, Nature, 409, 159
Bonnor, W. B. 1956, MNRAS, 116,351
Chandrasekhar, S., & Fermi, E. 1953, ApJ, 118, 113
Cohen, R. J., Rowland, P. R., & Blair, M. M. 1984, MNRAS, 210, 425
Ebert, R. 1955, Z. Astrophys., 37, 222
Fiege, J. D., & Pudritz, R. E. 2000, ApJ, 544, 830
Harvey, D. W. A., Wilner, D. J., Lada, C. J., Myers, P. C., Alves, J. ;., & Chen, H. 2001, ApJ, 563, 903.
Henning, T., Wolf, S., Launhardt, R., & Waters, R. 2001, ApJ, 561, 871
Houde, M. 2004, ApJ, 616, L111
Jones, T. J. & Amini, H. 2003, AJ, 125, 1418
Larson, R. B. 1969, MNRAS, 145, 271
Matsumoto, T., & Tomisaka, K. 2004, ApJ, 616, 266
Momose, M., Tamura, M., Kameya, O., Greaves, J. S., Chrysostomou, A., Hough, J. H., & Morino, J.-I. 2001, ApJ, 555, 855

Ménard, F., & Duchêne, G. 2004, A&A, 425, 973
Nakano, T., Nishi, R., & Umebayashi, T. 2002, ApJ, 573, 199
Ostriker, E. C., Stone, J. M., & Gammie, C. F. 2001, ApJ, 546, 980
Padoan, P., Goodman, A., Draine, B. T., Juvela, M., Nordlund, Å., Rögnvaldsson, Ö. E. 2001, ApJ, 559, 1005
Racca, G., Gómez, M., & Kenyon, S. J. 2002, AJ, 124, 2178
Strom, K. M., Strom, S. E., Wolff, S. C., Morgan, J., & Wenz, M. 1986, ApJS, 62, 39
Tamura, M. & Sato, S. 1989, AJ, 98, 1368
Vallée, J. P., Greaves, J. S., & Fiege, J. D. 2003, ApJ, 588, 910
Vrba, F. J., Luginbuhl, C. B., Strom, S. E., Strom, K. M., & Heyer, M. H. 1986, AJ, 92, 633
Vrba, F. J., Strom, S. E., & Strom, K. M. 1988, AJ, 96, 680
Wolf, S., Launhardt, R., & Henning, T. 2003, ApJ, 592, 233